ISSN 1063-7761, Journal of Experimental and Theoretical Physics, 2019, Vol. 129, No. 3, pp. 426–437. © Pleiades Publishing, Inc., 2019.
Russian Text © The Author(s), 2019, published in Zhurnal Eksperimental'noi i Teoreticheskoi Fiziki, 2019, Vol. 156, No. 3, pp. 507–520.

ELECTRONIC PROPERTIES OF SOLID

# Ground-State Fermion Parity and Caloric Properties of a Superconducting Nanowire

**V. V. Val'kov[a,*], V. A. Mitskan[a], and M. S. Shustin[a]**

[a] *Kirensky Institute of Physics, Federal Research Center KSC, Siberian Branch, Russian Academy of Sciences, Akademgorodok, Krasnoyarsk, 660036 Russia*

**e-mail: vvv@iph.krasn.ru*

Received October 17, 2018; revised March 7, 2019; accepted April 5, 2019

**Abstract**—The ground-state structure and fermion parity have been determined for a semiconductor nanowire with a strong Rashba spin–orbit interaction and proximity-induced superconductivity placed in an external magnetic field under periodic boundary conditions. Allowance for the open boundaries is shown to cause the topologically nontrivial parameter region to be partitioned into a set of subregions with a different ground-state fermionic parity. This peculiarity is related to the emergence of edge modes with nonmonotonically changing excitation energies in the system as its parameters change. At the quantum transition point, at which the ground-state fermionic parity changes, the edge-mode energy is zero. The magneto- and electrocaloric effects are shown to be effective characteristics that allow the series of quantum transitions in an open nanowire to be identified experimentally. These effects at low temperatures exhibit an anomalous behavior in the parameter region for which topologically stable Majorana modes are realized in long nanowires.

**DOI:** 10.1134/S1063776119080144

## 1. INTRODUCTION

In recent years, Majorana modes (MMs) have attracted considerable interest of the world scientific community owing to the prediction of the possibility of their detection in condensed matter [1–4]. In solid-state physics MMs are excitations whose characteristics in real space are distinctly nonlocal. Systems containing Majorana modes have a degenerate ground state. A consequence of this is, first, the possibility of the realization of a nontrivial topological ground-state structure [5–7]. Second, if the degenerate ground state is separated from the first excited one by a significant energy gap, then MMs are stable with respect to minor local perturbations. The aforesaid determines the interest in MMs as promising objects for the creation of a quantum computer protected from decoherence. Fundamentally, the interest in the Majorana problematics stems for the necessity of understanding and detecting the properties of condensed matter attributable to their nontrivial topological characteristics.

At present, it has been established that the topological phases of systems of noninteracting fermions can be classified from symmetry considerations [8–10]. Time-reversal, electron–hole, chiral, and mirror symmetries are examples of nonlocal symmetries characterizing the topological phases. For a given set of nonlocal symmetries and a certain spatial dimension the states of a fermion system (assuming the presence of a gap in the energy spectrum) break up into a set of topologically nonequivalent classes distinguished by the topological indices. Topologically protected gapless excitations, in particular, MMs, are realized at the interface between semi-infinite media with different values of these indices.

The classification of topological phases is complicated significantly when the interaction between fermions is taken into account. The latter can lead both to the induction of new topological phases and to a reduction in the number of nonequivalent topological states of the system. For example, using a model one-dimensional system of symmetry class BDI as an example, it was shown in [11] that the topological classification could be reduced using the $\mathbb{Z}$ invariant to a classification based on the $\mathbb{Z}_8$ topological index. Subsequently, this result was obtained by other methods using the formalism of Green's functions [12, 13], the scattering matrix [14], and a nonlinear sigma model [15, 16]. At the same time, the ways of classifying the topological phases of quasi-one-dimensional systems with an interaction were proposed [16–22]. The result obtained in [16] is important for this study. It demonstrates that the $\mathbb{Z}_2$ topological classification of systems of noninteracting fermions is stable with respect to the inclusion of four-fermion interactions in the system.

The solid-state systems in which MMs can be realized are quite varied. In the pioneering papers [23, 24] the existence of such quasi-particle excitations was

predicted in the vortex cores of two-dimensional chiral superconductors [23] and at the ends of quantum wires with proximity-induced superconductivity [24]. In both models the superconducting pairings had a *p*-wave symmetry. Later on, it was pointed out in [25] that *p*-wave superconductivity could be achieved in real systems through the joint realization of induced *s*-wave superconductivity, a strong spin-orbit interaction, and external fields. Following this idea, various hybrid structures containing an *s*-wave superconductor, 2D topological insulators [26], and semiconductor nanowires with a strong Rashba spin–orbit interaction [27, 28] being studied in this paper were considered. Note that systems in which the realization of Majorana modes is possible through internal interactions are also considered [29–32].

Among the presented systems, semiconductor nanowires with induced *s*-wave superconductivity and an external magnetic field (hereafter superconducting nanowires) are currently being studied most actively. The popularity of these systems is related, first, to the ease of their fabrication: epitaxially grown InAs or InSb semiconductors with a strong Rashba spin–orbit interaction and large *g*-factors ($g_{\mathrm{InAs}} \sim 10$–$25$ [33] and $g_{\mathrm{InSb}} \sim 20$–$70$ [34]) as well as standard Al-type BCS superconductors, whose thin layers (5–10 nm) are epitaxially deposited on the nanowire surface (see, e.g., [35]), are usually investigated. The second fact responsible for the popularity of superconducting nanowires is that the conditions and algorithms of quantum computations with MMs have been considered in detail for them [1, 36–39]. Note that the possibility of MM realization was also predicted for chains of magnetic atoms [40, 41] and nanowires without an external magnetic field [42, 43]. However, such systems are currently either speculative or poorly studied experimentally.

Most experimental studies of the manifestations of topologically nontrivial phases and MMs in superconducting nanowires are based on an analysis of their transport characteristics. For example, the emergence of MMs in such systems was confirmed experimentally by measuring the peak in the differential conductance at zero voltage [44, 45]. However, the question of whether the interpretation of the available experimental data concerning the detection of Majorana states in superconducting wires is unambiguous remains incompletely resolved [46–48]. It emerged in the course of theoretical studies that a consistent description of the existing experiments requires taking into account a number of nanowire properties, such as the tunneling between the wire and the superconducting substrate [49], the anisotropy of the wire *g*-factor [50], the electron–electron interactions [51, 52], the presence of disorder [53, 54], the multiband effects [55, 56], and the system's finite sizes [57–62].

The following conclusions are an overall picture of the investigation of electron–electron interaction effects in a nanowire [51, 52]: electron–electron interactions, on the one hand, reduce the gap in the system's bulk spectrum, thereby reducing its topological protectability, but, on the other hand, increase the range of parameters at which a topological phase can be realized. A similar conclusion holds for a system with disorder [53, 54]: relatively weak disorder does not destroy the topological phase in the system and the Majorana modes are not localized. In this case, allowance for the strong electron–electron interaction or strong disorder can lead to either the induction or the disappearance of topological states, depending on the system's parameters. The topological phase diagram is also significantly enriched by a joint examination of the electron–electron interaction, disorder, and multiband effects [55, 56, 63]. Note that, at present, the possibility of an effective representation of the ground state for nanowires with electron–electron interactions as matrix product states [20–22], which is convenient for a symmetry analysis of topological phases, is deemed universally recognized. In this case, an explicit form of the ground-state wave function for a superconducting nanowire (to be more precise, for its effective version—the Kitaev chain model [24]) was obtained only for an isolated, very narrow set of parameters [64, 65].

Among the studies of the finite-size effects of quantum wires in which MMs can be realized we can distinguish [57–62]. In particular, the oscillatory behavior of the splitting energy between the ground and first excited states as a function of the chain length and parameters, which is important for this study, was discussed in [60, 61]. Later on, it was shown for the model of a finite Kitaev chain in [62] that the minimum excitation energy oscillations correspond to a series of quantum transitions accompanied by a change in the ground-state fermion parity.

If we sum up the aforesaid, then we can see that searching for effects related to the existence of MMs in superconducting nanowires is still topical at present. Such effects must be stable to the introduction of disorder into the system, allowance for the electron–electron interactions, and a change in the system's spatial sizes. In this paper we show that if the parameters of a fairly short nanowire correspond to the conditions of MM realization in an infinite chain, then a change in the external magnetic field or electrostatic potential can be accompanied by a series of magneto- and electrocaloric anomalies. In the absence of disorder, the magnetocaloric effect is briefly considered in [66], where the caloric anomalies are demonstrated to be stable with respect to joint allowance for the weak single-site and intersite Coulomb correlations and diagonal disorder. The structure of the many-body ground state of a nanowire in a closed geometry is also

considered in [66]. The connection between the conditions for the realization of a topologically nontrivial phase and negative ground-state fermion parity is demonstrated explicitly.

The presentation of our results is organized as follows. The model of a semiconductor nanowire with proximity-induced superconductivity and electron–electron interactions is described in Section 2. The structure of the ground state of a closed nanowire is determined in Section 3. The latter is achieved by using the relationship between the $\mathbb{Z}_2$ topological invariant and ground-state fermionic parity. Section 4 is devoted to analyzing the ground-state fermionic parity for an open nanowire, while the magneto- and electrocaloric effects are discussed in Section 5. Special attention is given to an analysis of these properties at parameters corresponding to a nontrivial value of the system's $\mathbb{Z}_2$ invariant. Next we discuss the stability of the previously considered characteristics with respect to the presence of relatively weak electron correlations and disorder in the system and to a change in the system's sizes (Section 6).

## 2. THE MODEL OF A SUPERCONDUCTING NANOWIRE WITH ELECTRON-ELECTRON INTERACTIONS

We will consider a semiconductor InSb nanowire with a thin aluminum layer (3–5 nm) epitaxially deposited on its surface, which is responsible for the induction of superconductivity in the system. We will take into account the presence of a strong Rashba spin–orbit interaction and repulsive electron–electron interactions with intensities $U$ and $V$ in the nanowire. The Hamiltonian of such a system in the tight-binding approximation is [51]

$$\mathcal{H} = \sum_{l,\sigma}\left[\xi_\sigma a_{l\sigma}^\dagger a_{l\sigma} - \frac{t}{2}\left(a_{l\sigma}^\dagger a_{l+1\sigma} + a_{l+1\sigma}^\dagger a_{l\sigma}\right)\right]$$
$$+ \sum_l\left[\Delta a_{l\uparrow}a_{l\downarrow} - \frac{\alpha}{2}(a_{l\uparrow}^\dagger a_{l+1\downarrow} - a_{l\downarrow}^\dagger a_{l+1\uparrow}) + \text{H.c.}\right] \quad (1)$$
$$+ \sum_l (U\hat{n}_{l\uparrow}\hat{n}_{l\downarrow} + V\hat{n}_l\hat{n}_{l+1}),$$

where the terms in the first sum describe a one-dimensional system of fermions with the hopping integral $t/2$ and a spin-projection-dependent fermion energy at one site (measured from the chemical potential $\mu$),

$$\xi_\sigma = \epsilon_0 - \mu + \eta_\sigma h, \quad h = \frac{1}{2}g\mu_B H,$$

$g$ is the Lande factor, $\mu_B$ is the Bohr magnetron, $H$ is the external magnetic field, $a_{l\sigma}(a_{l\sigma}^\dagger)$ is the annihilation (creation) operator of a fermion at site $l$ and with spin projection $\sigma = \uparrow, \downarrow$, $\eta_\uparrow = 1$, $\eta_\downarrow = -1$. The terms related to the presence (due to the proximity effect) of a superconducting pairing potential with amplitude $\Delta$ and the terms attributable to the Rashba spin–orbit interaction with parameter $\alpha$ are presented in the second sum of the Hamiltonian. The last terms of the Hamiltonian correspond to allowance for the single-site ($U$) and intersite ($V$) Coulomb interactions between fermions. The electron number operator at a site is $\hat{n}_l = \hat{n}_{l\uparrow} + \hat{n}_{l\downarrow}$, $\hat{n}_{l\sigma} = a_{l\sigma}^\dagger a_{l\sigma}$. In all sections, except for Section 6, we will set $U = V = 0$. Note that the anomalously high $g$-factor in the system ($g \simeq 50$) is important from the standpoint of the possibility of MM realization, because the application of magnetic fields ~1 tesla will allow the realization of a topologically nontrivial phase to be achieved in the system. Since the caloric characteristics of the system were not considered in most papers, we will restrict ourselves to a semi-quantitative analysis at a chosen ratio of parameters, $\alpha/|t| \simeq 0.2$ and $\Delta/|t| \simeq 0.3$.

## 3. STRUCTURE OF THE GROUND STATE OF A CLOSED NANOWIRE IN TOPOLOGICALLY TRIVIAL AND NONTRIVIAL PHASES

The Hamiltonian of a superconducting nanowire (1) has an electron–hole symmetry, is characterized by broken time-reversal symmetry, and refers to the symmetry class $D$. Its topological properties are classified by means of the $\mathbb{Z}_2$ invariant [9]. A form of this invariant (Majorana number $\mathcal{M}$) expressed via the ground-state fermionic parity $P(\mathcal{H}(N))$ of a closed nanowire was proposed in [24]:

$$P(\mathcal{H}(N_1 + N_2)) = \mathcal{M}P(\mathcal{H}(N_1))P(\mathcal{H}(N_2)). \quad (2)$$

It follows from the presented definition that for a chain with an even number of sites the topological index $\mathcal{M}$ coincides with the fermionic parity of such a closed nanowire. The wave function that describes a superposition of states with an even (odd) number of fermions corresponds to $\mathcal{M} = 1$ ($\mathcal{M} = -1$).

The formation of negative fermionic parity is related to the structure of the Hamiltonian at singular points of the Brillouin zone. In the case under consideration, this follows from the fact that in the quasi-momentum representation the Hamiltonian (1) breaks up into a direct sum of quadratic forms:

$$\mathcal{H} = \hat{h}(0) + \hat{h}(\pi) + \sum_{0<k<\pi}\hat{r}(k), \quad (3)$$

each of which acts in its invariant subspace. In Eq. (3) the form $\hat{r}(k) = \hat{h}(k) + \hat{h}(-k)$ is represented by a combination of the form $\hat{h}(k)$ even in quasi-momentum:

$$\hat{h}(k) = \sum_\sigma \xi_{k\sigma}\hat{n}_{k\sigma}$$
$$+ (i\alpha_k a_{k\downarrow}^\dagger a_{k\uparrow} + \Delta a_{k\uparrow}a_{-k\downarrow} + \text{H.c.}), \quad (4)$$

where

$$\xi_{k\sigma} = \xi_k + \eta_\sigma h, \quad \xi_k = t\cos k - \mu, \quad \alpha_k = \alpha \sin k.$$

The extraction of the forms

$$\hat{h}(0) = \sum_\sigma \xi_{0\sigma}\hat{n}_{0\sigma} + (\Delta a_{0\uparrow}a_{0\downarrow} + \text{H.c.}),$$
$$\hat{h}(\pi) = \sum_\sigma \xi_{\pi\sigma}\hat{n}_{\pi\sigma} + (\Delta a_{\pi\uparrow}a_{\pi\downarrow} + \text{H.c.}), \quad (5)$$
$$\hat{n}_{0\sigma} = a^\dagger_{0\sigma}a_{0\sigma}, \quad \hat{n}_{\pi\sigma} = a^\dagger_{\pi\sigma}a_{\pi\sigma}$$

from the general summation in the Hamiltonian (3) is related to three factors. The first factor follows from the fact that the points $k = 0$ and $k = \pi$ are symmetric in the sense that $k = -k + G$, where $G$ is the reciprocal lattice vector. The second factor is determined by the fact that the spin–orbit interaction becomes zero at these points. The third and most important factor stems from the fact that the change in the ground-state fermion parity of a quantum wire as the system's parameters (for example, the magnetic field) change is determined only by the change in the structure of the ground state of the forms $\hat{h}(0)$ and $\hat{h}(\pi)$.

Obviously, among the four eigenvectors of the form $\hat{h}(0)$ (and similarly the form $\hat{h}(\pi)$), two vectors correspond to a state with one fermion:

$$|F_{Q\sigma}\rangle = a^\dagger_{Q\sigma}|0\rangle, \quad Q = 0,\pi, \quad \sigma = \uparrow,\downarrow. \quad (6)$$

The other two eigenvectors are a linear combination of the vectors corresponding to states with an even number of fermions:

$$|\Phi_{Q,\pm}\rangle = \hat{R}_{Q,\pm}|0\rangle,$$
$$\hat{R}_{Q,\pm} = A_{Q,\pm} + B_{Q,\pm}a^\dagger_{Q\downarrow}a^\dagger_{Q\uparrow}. \quad (7)$$

In these expressions the vacuum state of the entire system of fermions is denoted by $|0\rangle$.

The relation between the energy $E^F_{Q\downarrow} = \xi_{Q\downarrow}$ of the single-fermion state $|F_{Q\downarrow}\rangle$ and the energy $E^\Phi_{Q,-} = \xi_Q - \sqrt{\xi^2_Q + |\Delta|^2}$ of the state $|\Phi_{Q,-}\rangle$ is important for the subsequent analysis. From the requirement that the energy of the state $|F_{0\downarrow}\rangle$ be less than the energy of the state $|\Phi_{0,-}\rangle$ we obtain a condition for the realization of a single-fermion state at $k = 0$:

$$h > \sqrt{(t-\mu)^2 + |\Delta|^2}. \quad (8)$$

Examining an analogous condition for $k = \pi$ leads to the inequality

$$h > \sqrt{(t+\mu)^2 + |\Delta|^2}. \quad (9)$$

If it holds, then the state with the quasi-momentum $k = \pi$ is filled with strictly one electron.

It follows from the quadratic form $\hat{r}(k)$ that its eigenvector corresponding to zero total quasi-momentum and the lowest energy can be represented as

$$|\psi_k\rangle = \hat{R}_k|0\rangle, \quad (10)$$

where the operator generating a superposition of states with an even number of fermions is defined by the expression

$$\hat{R}_k = A_k + B_k a^\dagger_{-k\downarrow}a^\dagger_{k\uparrow} + C_k a^\dagger_{k\downarrow}a^\dagger_{-k\uparrow} + D_k a^\dagger_{-k\uparrow}a^\dagger_{k\uparrow} + F_k a^\dagger_{-k\downarrow}a^\dagger_{k\downarrow} + G_k a^\dagger_{-k\downarrow}a^\dagger_{k\uparrow}a^\dagger_{k\downarrow}a^\dagger_{-k\uparrow}. \quad (11)$$

The coefficients $A_k$, $B_k$, ..., $G_k$ appearing here and six energy levels are determined from the solution of the eigenvalue problem $H^{\text{ev}}_k \vec{X}_k = E_k \vec{X}_k$, where

$$H^{\text{ev}}_k = \begin{pmatrix} 0 & \Delta & \Delta & 0 & 0 & 0 \\ \Delta^* & 2\xi_k & 0 & i\alpha_k & -i\alpha_k & \Delta \\ \Delta^* & 0 & 2\xi_k & -i\alpha_k & i\alpha_k & \Delta \\ 0 & -i\alpha_k & i\alpha_k & \xi_{k\uparrow} & 0 & 0 \\ 0 & i\alpha_k & -i\alpha_k & 0 & \xi_{k\downarrow} & 0 \\ 0 & \Delta^* & \Delta^* & 0 & 0 & 4\xi_k \end{pmatrix},$$
$$\vec{X}_k = (A_k, B_k, C_k, D_k, F_k, G_k)^T.$$

Our analysis of the eigenvectors of the quadratic forms of the Hamiltonian shows that the ground-state wave function of a closed superconducting nanowire with an even number of sites can be represented in one of four qualitatively different forms. Each form of the ground-state wave function is realized in its own parameter region. These regions are shown in Fig. 1 at $\Delta = 0.35|t|$. The structure of the ground-state wave function in these regions is specified by the expressions

$$|\Psi^{(\text{I})}\rangle = (\hat{R}_{0,-})(\hat{R}_{\pi,-})\left(\prod_{0<k<\pi}\hat{R}_k\right)|0\rangle,$$
$$|\Psi^{(\text{II})}\rangle = (\hat{R}_{0,-})(a^\dagger_{\pi\downarrow})\left(\prod_{0<k<\pi}\hat{R}_k\right)|0\rangle,$$
$$|\Psi^{(\text{III})}\rangle = (a^\dagger_{\pi\downarrow})(\hat{R}_{\pi,-})\left(\prod_{0<k<\pi}\hat{R}_k\right)|0\rangle, \quad (12)$$
$$|\Psi^{(\text{IV})}\rangle = (a^\dagger_{0\downarrow})(a^\dagger_{0\uparrow})\left(\prod_{0<k<\pi}\hat{R}_k\right)|0\rangle.$$

It is clearly seen from the above structure of the ground-state wave function in various regions of the phase diagram that the ground-state fermion parity of a nanowire is determined only by filling of the states with the quasi-momenta $k = 0$ and $k = \pi$. The wave functions $|\Psi^{(\text{I})}\rangle$ and $|\Psi^{(\text{IV})}\rangle$ are represented as a superposition of states with an even number of fermions. Accordingly, the Majorana number is $\mathcal{M} = +1$. For the wave functions $|\Psi^{(\text{II})}\rangle$ and $|\Psi^{(\text{III})}\rangle$ states with an odd

number of fermions enter into the superposition. Therefore, at the system's parameters falling into regions II and III the ground state of the quantum wire under consideration has a negative fermionic parity and a topologically nontrivial phase with the Majorana number $\mathcal{M} = -1$ is realized in the nanowire. Note that the Majorana number was calculated previously via the Pfaffian of the Bogoliubov–de Gennes matrix in the representation of Majorana operators [24]. Both approaches yield the same result, but the structure of the ground-state wave function manifests itself clearly in the representation (12).

## 4. SERIES OF QUANTUM TRANSITIONS IN AN OPEN NANOWIRE

The reasoning given in the previous section referred to a chain in a closed geometry. In this case, the Majorana number $\mathcal{M}$ is directly related to the Zak–Berry phase [7, 67]. This allows $\mathcal{M}$ to be considered as the $\mathbb{Z}_2$ invariant that classifies different topological phases: at $\mathcal{M} = 1$ ($\mathcal{M} = -1$) a closed chain is in a trivial (nontrivial) topological phase. When an open nanowire is considered, the connection of the ground-state fermion parity with topological characteristics is lost.

Let us assume below that the parameter region for which a closed nanowire is in a topologically nontrivial phase is the topologically nontrivial parameter region (TNPR). In the case of fairly long open chains, topologically protected Majorana modes are realized in the entire TNPR. The Majorana polarization $\mathcal{P}$ was introduced [57, 58] for an efficient search for the conditions of MM realization when considering a chain in an open geometry. For the purposes of our subsequent analysis, it is convenient to represent this quantity as follows:

$$\mathcal{P} = \frac{2\left|\sum_{l\sigma}{}' u^*_{l\sigma,0}v_{l\sigma,0}\right|}{\sum_{l\sigma}{}'(u^2_{l\sigma,0} + v^2_{l\sigma,0})} = \frac{\left|\sum_{l\sigma}{}'(w^2_{l\sigma,0} - z^2_{l\sigma,0})\right|}{\sum_{l\sigma}{}'(w^2_{l\sigma,0} + z^2_{l\sigma,0})}. \quad (13)$$

Here, the summation is over the sites $l$ belonging only to the left (or only to the right) half of the chain, while $w_{l\sigma,0}$ and $z_{l\sigma,0}$ are the coefficients of the expansion of the self-adjoint operators $b' = (\alpha_0 + \alpha_0^\dagger)/2$ and $b'' = (\alpha_0^\dagger - \alpha_0)/2$ in terms of the single-site Majorana operators $\gamma_{Al\sigma}$ and $\gamma_{Bl\sigma}$:

$$\gamma_{Al\sigma} = \frac{1}{2}(e^{i\theta/2}a^\dagger_{l\sigma} + e^{-i\theta/2}a_{l\sigma}),$$

$$\gamma_{Bl\sigma} = \frac{i}{2}(e^{i\theta/2}a^\dagger_{l\sigma} - e^{-i\theta/2}a_{l\sigma}), \quad (14)$$

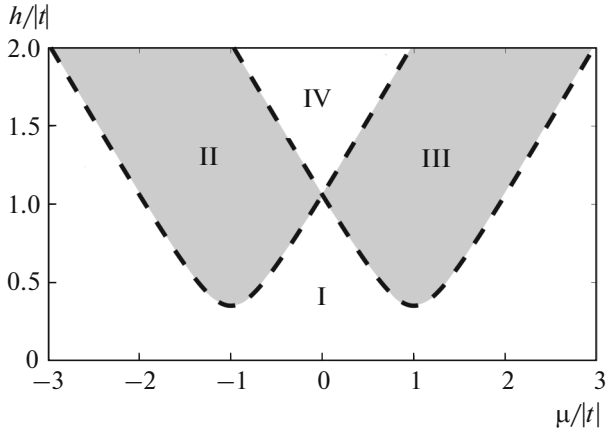


**Fig. 1.** Topological phase diagram for a closed nanowire in chemical potential–external magnetic field variables. Regions II, III and I, IV correspond to nontrivial ($\mathcal{M} = -1$) and trivial topological phases, respectively. The superconducting pairing parameters $\Delta = 0.35|t|$ (in a closed geometry the phase diagram does not depend on $\alpha$).

$$b' = \sum_{l=1;\sigma}^{N} w_{l\sigma,0}\gamma_{Al\sigma}, \quad b'' = \sum_{l=1;\sigma}^{N} z_{l\sigma,0}\gamma_{Bl\sigma}.$$

Here, $\theta$ is the phase of the superconducting order parameter $\Delta = |\Delta|e^{i\theta}$. The real-valued functions $w_{l\sigma,0}$ and $z_{l\sigma,0}$ can be expressed via the coefficients of the Bogoliubov transformation for a quasi-particle $\alpha_0$ corresponding to the mode with minimum energy $\varepsilon_0$:

$$w_{l\sigma,0} = e^{-i\theta/2}(u_{l\sigma,0} + v_{l\sigma,0}),$$
$$z_{l\sigma,0} = e^{-i\theta/2}(u_{l\sigma,0} - v_{l\sigma,0}), \quad (15)$$
$$\alpha_m = \sum_{l,\sigma}(u^*_{l\sigma,m}a_{l\sigma} + v_{l\sigma,m}a^\dagger_{l\sigma}).$$

The coefficients $u_{l\sigma,0}$ and $v_{l\sigma,0}$ form the eigenvectors of the Bogoliubov– de Gennes matrix:

$$H = \begin{pmatrix} A_{\uparrow\uparrow} & A_{\uparrow\downarrow} & B_{\uparrow\uparrow} & B_{\uparrow\downarrow} \\ A^\dagger_{\uparrow\downarrow} & A_{\downarrow\downarrow} & -B^T_{\uparrow\downarrow} & B_{\downarrow\downarrow} \\ -B^*_{\uparrow\uparrow} & -B^*_{\uparrow\downarrow} & -A^*_{\uparrow\uparrow} & -A^*_{\uparrow\downarrow} \\ B^\dagger_{\uparrow\downarrow} & -B^*_{\downarrow\downarrow} & -A^T_{\uparrow\downarrow} & -A^*_{\downarrow\downarrow} \end{pmatrix} \quad (16)$$

with the eigenvalue $\varepsilon_0$. The following components of the Hermitian ($A_{\sigma\sigma'}$) and antisymmetric ($B_{\sigma\sigma'}$) matrices are nonzero here:

$$(A_{\uparrow\downarrow})_{l,l+1} = -(A_{\uparrow\downarrow})_{l+1,l} = -\alpha/2,$$
$$(B_{\uparrow\downarrow})_{l,l} = -\Delta, \quad (17)$$
$$(A_{\sigma\sigma})_{l,l} = \epsilon_0 - \mu + \eta_\sigma h, \quad (A_{\sigma\sigma})_{l,l+1} = -t/2.$$

The convenience of introducing the Majorana polarization $\mathcal{P}$ is that $\mathcal{P} = 0$ when considering long

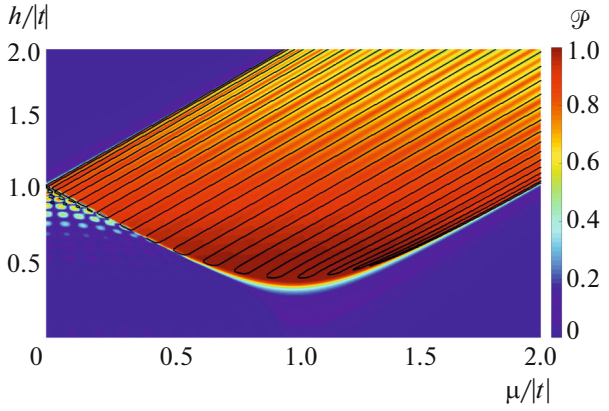


**Fig. 2.** (Color online) Dependence of the Majorana polarization $\mathcal{P}$ on magnetic field $h$ and chemical potential $\mu$ for an open chain of 30 sites with an induced superconducting pairing potential ($\Delta = 0.35|t|$) and a Rashba spin–orbit interaction ($\alpha = 0.22|t|$). The black lines mark the zero modes.

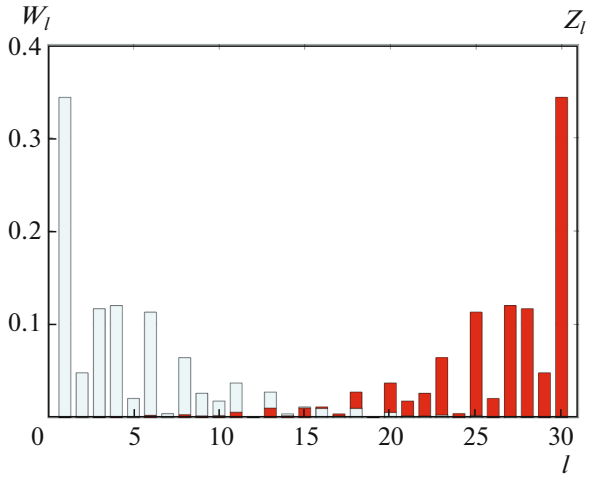


**Fig. 3.** (Color online) Distributions $W_l = |\sum_\sigma w_{l\sigma,0}|^2$ and $Z_l = |\sum_\sigma z_{l\sigma,0}|^2$ at $h = 0.8|t|$ and $\mu = 0.5|t|$ (corresponds to the TNPR, $\mathcal{P} = 0.91$). The behavior of $Z_l$ is similar to the behavior of $W_l$ under the substitution $l \to N - l + 1$.

chains outside the TNPR and $\mathcal{P} = 1$ inside this region. The equality $\mathcal{P} = 1$ implies the absence of an overlap between the $w_{l\sigma,0}$ and $z_{l\sigma,0}$ distributions and corresponds to the localization of these functions near different edges of the chain. It is easy to show that this condition also corresponds to the electrical and spin neutrality of a Majorana excitation. For example, the variation of the electron and spin density distributions,

$$\begin{aligned}\delta n_{l\sigma} &= \langle 1|a_{l\sigma}^\dagger a_{l\sigma}|1\rangle - \langle 0|a_{l\sigma}^\dagger a_{l\sigma}|0\rangle \\ &= |u_{l\sigma,0}|^2 - |v_{l\sigma,0}|^2 = w_{l\sigma,0}z_{l\sigma,0},\end{aligned} \tag{18}$$

and

$$\begin{aligned}\delta s_l^z &= \frac{1}{2}\sum_\sigma \eta_\sigma w_{l\sigma,0}z_{l\sigma,0}, \\ \delta s_l^x &= \frac{1}{2}\sum_\sigma w_{l\sigma,0}z_{l\bar{\sigma},0}\end{aligned} \tag{19}$$

as the superconducting nanowire passes from the ground state $|0\rangle$ to the state with a filled Majorana mode $|1\rangle = \alpha_0^\dagger|0\rangle$ is zero in the described case. Thus, the observation of Majorana modes in long nanowires by measuring the spin and electron densities is impossible.

As the chain length decreases, the $w_{l\sigma,0}$ and $z_{l\sigma,0}$ distributions inside the TNPR begin to overlap. The degree of such overlapping can be depicted by constructing a map of the Majorana polarization $\mathcal{P}$ (see Fig. 2). Edge modes (in the sense given in [68]) with overlapping $w_{l\sigma,0}$ and $z_{l\sigma,0}$ distributions are realized in the parametric regions in which $0 < \mathcal{P} < 1$ (Fig. 3). In general, the energy of such modes is nonzero, but gapless excitations can emerge in the system at certain model parameters. These excitations are realized not in a wide parametric region, but on the special parametric lines displayed in Figs. 2 and 4. It is worth noting that, for the latter reason, such gapless excitations are of no interest from the viewpoint of quantum computations. However, below we will present an approach that allows the topologically nontrivial parameter region to be efficiently determined when investigating a short open chain.

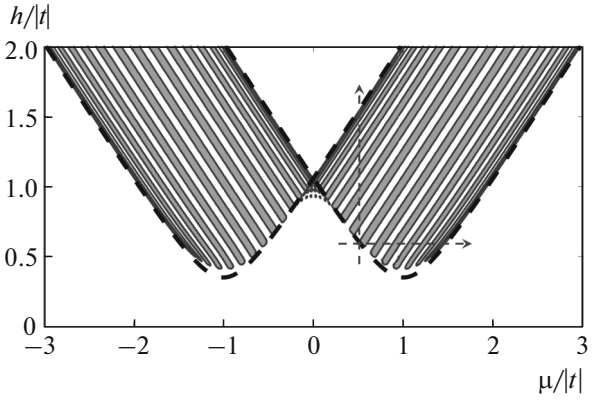


**Fig. 4.** Phase diagram for an open nanowire ($N = 30$) at $\Delta = 0.35|t|$ and $\alpha = 0.22|t|$. The hatched regions correspond to the parameters for which the ground state contains partial contributions with an odd number of fermions. The lines for the points of which a quantum phase transition is realized are the boundaries of these regions. The dashed lines indicate the boundaries at which a topologically nontrivial phase is realized for a closed nanowire (see Fig. 1). The change in parameters along the blue dashed lines with arrows corresponds to the field dependences in Fig. 5 (the vertical and horizontal dashes correspond to Figs. 5a and 5b, respectively).

From the standpoint of the eigenstates of the Hamiltonian (1), the emergence of a zero mode on the special parametric lines implies ground-state degeneracy. Significantly, when passing such parametric points, two states with different fermion parities alternate as the ground state and quantum transitions are realized in the system. Thus, the lines of zero modes in this system are the parametric lines of quantum critical points. For an open nanowire the result of calculating the fermionic parity index $P$ allows the system's phase diagram presented in Fig. 4 to be constructed. The value of $P$ can be found as the sign of the Pfaffian of the Bogoliubov–de Gennes matrix (16) brought to an antisymmetric form:

$$P = \mathrm{sgn}(\mathrm{Pf}(\tilde{H})), \quad \tilde{H} = R^T H \Lambda R,$$
$$R = \begin{pmatrix} \hat{I} & -i\hat{I} \\ \hat{I} & i\hat{I} \end{pmatrix}, \quad \Lambda = \begin{pmatrix} \hat{0} & \hat{I} \\ \hat{I} & \hat{0} \end{pmatrix}, \tag{20}$$

where $\hat{I}$ is a $2N \times 2N$ unit matrix.

$P = -1$, at which the partial contributions to the ground state contain an odd number of fermions, corresponds to the hatched regions in Fig. 4. The parametric lines for which the ground state is doubly degenerate and the minimum excitation energy is zero serve as the boundaries of these regions. The boundaries of the topological phases of a closed chain displayed in Fig. 1 are again represented by thick dashed lines. We see that the lines of zero modes can be realized both inside and outside the TNPR. When the nanowire length increases, the lines of change of the fermion parity disappear in the parametric region with $\mathcal{M} = 1$, while in the parameter region with $\mathcal{M} = -1$ their number grows and they form a quasi-continuum in the TNPR in the limit $N \to \infty$.

Thus, a peculiarity of the TNPR in a nanowire is the realization of a cascade of quantum transitions in it as the external parameters (the external magnetic field or voltage) change. Such a cascade can be efficiently detected using the observed characteristics. In particular, the spin and electron density redistributions (18) become nonzero for the parameters corresponding to these lines. However, the TNPR can apparently be detected most efficiently by measuring the magneto- and electrocaloric effects.

## 5. MAGNETO- AND ELECTROCALORIC ANOMALIES

The caloric effects, magnetic and electric, are known to be effective thermodynamic characteristics that allow the quantum transitions to be identified [69, 70]. These effects manifests themselves as a change in the system's temperature as the magnetic field or voltage changes adiabatically and are defined by the expressions

$$\left(\frac{\partial T}{\partial h}\right)_{S,\mu} = -T\left(\frac{\partial\langle M\rangle/\partial T}{C(T)}\right)_{\mu,h},$$
$$\left(\frac{\partial T}{\partial \mu}\right)_{S,h} = -T\left(\frac{\partial\langle N\rangle/\partial T}{C(T)}\right)_{\mu,h}, \tag{21}$$

where $\langle N\rangle$, $\langle M\rangle$, and $C(T)$ are the electron density, specific magnetization, and specific heat, respectively. It is quite easy to show that the quantities (21) have different signs in the right and left neighborhoods of the quantum critical point and diverge at these points at low temperatures. The first singularity is related to the change in the number of fermions and the ground-state spin structure during quantum transitions. Accordingly, $\langle N\rangle$ and $\langle M\rangle$ change at the quantum critical point abruptly at $T = 0$. At low, but finite temperatures the quantum phase transition is replaced by a crossover and, accordingly, the derivatives of these quantities with respect to the temperature have different signs in the neighborhoods of the critical point. To demonstrate the second singularity, let us rewrite the expressions for the specific heat and the derivatives $\partial\langle M\rangle/\partial T$ and $T\partial\langle N\rangle/\partial T$ as

$$\frac{\partial\langle N\rangle}{\partial T} = \frac{1}{2T^2}\sum_{m=1}^{2N} A_m \varepsilon_m f(\varepsilon_m/T)[1 - f(\varepsilon_m/T)],$$
$$\frac{\partial\langle M\rangle}{\partial T} = \frac{1}{2T^2}\sum_{m=1}^{2N} B_m \varepsilon_m f(\varepsilon_m/T)[1 - f(\varepsilon_m/T)], \tag{22}$$
$$C(T) = \frac{1}{T^2}\sum_{m=1}^{2N} \varepsilon_m^2 f(\varepsilon_m/T)[1 - f(\varepsilon_m/T)],$$

where

$$A_m = \sum_{l=1,\sigma}^{N} (|u_{l\sigma,m}|^2 - |v_{l\sigma,m}|^2),$$
$$B_m = \sum_{l=1,\sigma}^{N} \eta_\sigma (|u_{l\sigma,m}|^2 - |v_{l\sigma,m}|^2),$$

$f(\varepsilon_m/T)$ is the Fermi–Dirac function.

It can be seen from an examination of these expressions that at temperatures much lower than the characteristic gap of the bulk spectrum the edge modes with an oscillating excitation energy $\varepsilon_0$ make a major contribution to the functions $\partial\langle N\rangle/\partial T$, $\partial\langle M\rangle/\partial T$, and $C(T)$. An inverse dependence of the caloric effects (21) on minimum excitation energy $\varepsilon_0$ must be observed in the neighborhoods of the parametric lines of zero modes (because the system's specific heat $C(T) \propto \varepsilon_0^2$, while the increments $\partial\langle N\rangle/\partial T$ and $\partial\langle M\rangle/\partial T \propto \varepsilon_0$). Thus, at low temperatures the caloric effects must diverge at the quantum critical point and have a nearly zero value far from them. This behavior is displayed in Fig. 5. The dashed lines indicate the dependences of the caloric effects for a closed nanowire, in which the quantum transitions are accompanied by a change in

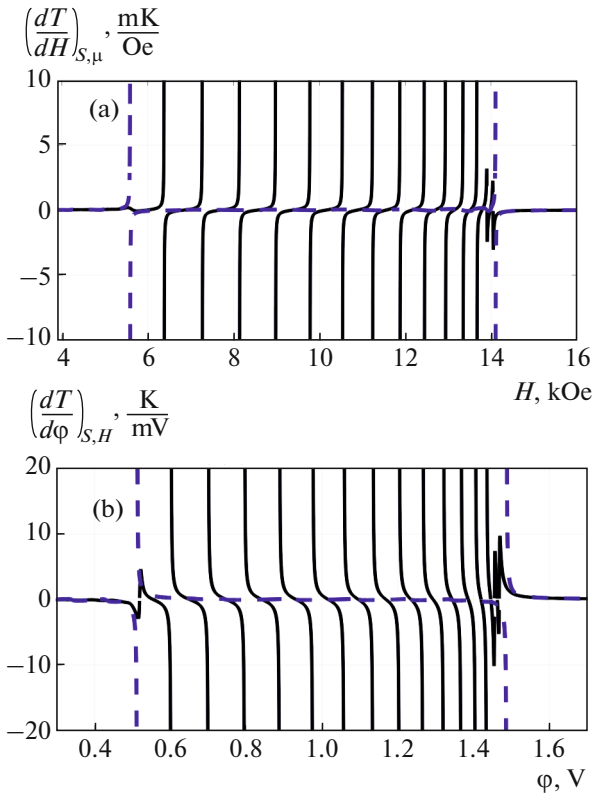


**Fig. 5.** (Color online) Field dependences of the magnetocaloric ($a$, $\mu/|t| = 0.5$) and electrocaloric ($b$, $h/|t| = 0.6$) effects. $T = 57$ mK, the remaining parameters correspond to Fig. 4. It can be seen from a comparison with Fig. 4 that the caloric effects exhibit an anomalous behavior in the TNPR.

the topological index $\mathcal{M}$. The solid lines represent the analogous dependences for an open nanowire.

It can be seen from Fig. 5 that the magnitudes of the magneto- and electrocaloric effects have bright features in the TNPR at low temperatures. The identification of these features can serve as a criterion for detecting the TNPR complementary to the already proposed ones in the literature (see, e.g., [2, 45, 71]).

## 6. STABILITY OF THE CALORIC ANOMALIES

In this section we demonstrate the stability of the series of magneto- and electrocaloric anomalies in the TNPR with respect to allowance for the electron–electron interactions, diagonal disorder, and changes in the system's sizes.

As was shown in [16], the classification of the topological phases of one-dimensional systems using the $\mathbb{Z}_2$ invariant is retained when four-fermion terms are added to the quadratic Hamiltonian. Accordingly, when studying the regions of realization of the system's topologically nontrivial phase described by the Hamiltonian (1) with nonzero single-site ($U > 0$) and intersite ($V > 0$) electron–electron interaction parameters, we still used the definition of the topological index (2). For example, the Majorana number $\mathcal{M}$ of a system with interactions was identified with the ground-state fermionic parity of the corresponding closed chain with an even number of sites. The spectral and thermodynamic peculiarities of the TNPR were analyzed numerically using the following two approaches.

In the first approach we used an exact diagonalization of the Hamiltonian for a chain with a small number of sites by means of which the low-energy branches of the Fermi excitation spectrum were found. The latter was done based on Lehmann's representation [72]:

$$-i\langle T_t \tilde{a}^\dagger_{l\sigma}(t)\tilde{a}_{l'\sigma'}(t')\rangle_\omega = \sum_{s=1}^{4^N-1}\left(\frac{(a^\dagger_{l\sigma})_{0s}(a_{l'\sigma'})_{s0}}{\omega - E_s + E_0 + i\delta} + \frac{(a_{l'\sigma'})_{0s}(a^\dagger_{l\sigma})_{0s}}{\omega + E_s - E_0 - i\delta}\right), \quad (23)$$

where $(a^\dagger_{l\sigma})_{s0} = \langle s|a^\dagger_{l\sigma}|0\rangle$. Here, $|0\rangle$ and $|s\rangle$ are the ground state and the $s$th excited eigenstate of the Hamiltonian (1), $E_0$ and $E_s$ are the energies of the corresponding states. In the absence of a Coulomb interaction, $2N$ transitions are known to be effective, for which the energies and the matrix elements $(a^\dagger_{l\sigma})_{m0}$ and $(a_{l\sigma})_{m0}$ are related to the excitation energies and the $u - v$ Bogoliubov coefficients:

$$E_m - E_0 = \varepsilon_m, \quad m = 1,\ldots,2N, \qquad |(a^\dagger_{l\sigma})_{m0}| = |u_{l\sigma,m}|, \quad |(a_{l\sigma})_{m0}| = |v_{l\sigma,m}|. \quad (24)$$

In the presence of a four-fermion interaction, in general, $2^{2N-1}$ matrix elements $(a^\dagger_{l\sigma})_{m0}$ and $(a_{l\sigma})_{m0}$ are nonzero. However, if $2N$ transitions can be chosen from these $2^{2N-1}$ transitions in such a way that the condition

$$\sum_{m=1}^{2N}(|(a^\dagger_{l\sigma})_{m0}|^2 + |(a_{l\sigma})_{m0}|^2) \cong 1,$$

is fulfilled, then relation (24) will also hold with a high accuracy after the substitution $u_{l\sigma,\,m}$, $v_{l\sigma,m}$, $\varepsilon_m \to \tilde{u}_{l\sigma,m}$, $\tilde{v}_{l\sigma,m}$, and $\tilde{\varepsilon}_m$. By $\tilde{u}_{l\sigma,m}$, $\tilde{v}_{l\sigma,m}$, and $\tilde{\varepsilon}_m$ we already mean the coefficients of the Bogoliubov $u - v$ transformation and the excitation energies obtained when considering the system in terms of the second method, namely in the generalized mean-field approximation [73, 74].

To analyze the system in this approximation, let us transform the four-fermion terms of the Hamiltonian (1) using the decoupling:

$$\begin{aligned} a^\dagger_{l\sigma}a^\dagger_{m\sigma'}a_{m\sigma'}a_{l\sigma} \to{}& \langle a^\dagger_{l\sigma}a_{l\sigma}\rangle a^\dagger_{m\sigma'}a_{m\sigma'} + \langle a^\dagger_{m\sigma'}a_{m\sigma'}\rangle a^\dagger_{l\sigma}a_{l\sigma} \\ &- \langle a^\dagger_{l\sigma}a_{m\sigma'}\rangle a^\dagger_{m\sigma'}a_{l\sigma} - \langle a^\dagger_{m\sigma'}a_{l\sigma}\rangle a^\dagger_{l\sigma}a_{m\sigma'} \\ &- \langle a^\dagger_{m\sigma'}a^\dagger_{l\sigma}\rangle^* a^\dagger_{l\sigma}a^\dagger_{m\sigma'} - \langle a^\dagger_{l\sigma}a^\dagger_{m\sigma'}\rangle a_{l\sigma}a_{m\sigma'}. \end{aligned} \quad (25)$$

In this case, the system's Hamiltonian in the Bogoliubov–de Gennes form can be written as

$$\mathscr{H} = \frac{1}{2}\mathbf{a}^{\dagger} \cdot H\mathbf{a}, \tag{26}$$

$$H = \begin{pmatrix} A_{\uparrow\uparrow} & A_{\uparrow\downarrow} & B_{\uparrow\uparrow} & B_{\uparrow\downarrow} \\ A^{\dagger}_{\uparrow\downarrow} & A_{\downarrow\downarrow} & -B^{T}_{\uparrow\downarrow} & B_{\downarrow\downarrow} \\ -B^{*}_{\uparrow\uparrow} & -B^{*}_{\uparrow\downarrow} & -A^{*}_{\uparrow\uparrow} & -A^{*}_{\uparrow\downarrow} \\ B^{\dagger}_{\uparrow\downarrow} & -B^{*}_{\downarrow\downarrow} & -A^{T}_{\uparrow\downarrow} & -A^{*}_{\downarrow\downarrow} \end{pmatrix}, \tag{27}$$

$\mathbf{a}^{\dagger} = (\mathbf{a}^{\dagger}_{\uparrow}, \mathbf{a}^{\dagger}_{\downarrow}, \mathbf{a}_{\uparrow}, \mathbf{a}_{\downarrow})$, $\mathbf{a}_{\sigma} = (a_{1\sigma}, ..., a_{N\sigma})$, and the matrices $A_{\sigma,\sigma'}$ and $B_{\sigma,\sigma'}$ have the following nonzero components dependent on the intensity of electron–electron interactions ($A_{\sigma\sigma} = A^{\dagger}_{\sigma\sigma}$ and $B_{\sigma\sigma} = -B^{T}_{\sigma\sigma}$):

$$\begin{aligned}
(A_{\sigma\sigma})_{l,l} &= \Delta\mu_l - \mu + \eta_{\sigma}h + U\langle a^{\dagger}_{l,\bar{\sigma}}a_{l,\bar{\sigma}}\rangle \\
&+ V\left(\sum_{\sigma'}\langle a^{\dagger}_{l-1,\sigma'}a_{l-1,\sigma'}\rangle + \langle a^{\dagger}_{l+1,\sigma'}a_{l+1,\sigma'}\rangle\right), \\
(A_{\sigma\sigma})_{l,l+1} &= -\frac{t}{2} - V\langle a^{\dagger}_{l\uparrow}a_{l+1,\uparrow}\rangle, \\
(A_{\uparrow\downarrow})_{l,l} &= -U\langle a^{\dagger}_{l\downarrow}a_{l,\uparrow}\rangle, \\
(A_{\uparrow\downarrow})_{l,l+1} &= -\frac{\alpha}{2} - V\langle a^{\dagger}_{l+1\downarrow}a_{l\uparrow}\rangle, \\
(A_{\uparrow\downarrow})_{l+1,l} &= \frac{\alpha}{2} - V\langle a^{\dagger}_{l+1\downarrow}a_{l\uparrow}\rangle^{*}, \\
(B_{\sigma\sigma})_{l,l+1} &= \frac{V}{2}\langle a^{\dagger}_{l\sigma}a^{\dagger}_{l+1\sigma}\rangle^{*}, \\
(B_{\uparrow\downarrow})_{l,l} &= -\Delta^{*} - \frac{U}{2}\langle a^{\dagger}_{l\downarrow}a^{\dagger}_{l\uparrow}\rangle^{*}, \\
(B_{\uparrow\downarrow})_{l,l+1} &= \frac{V}{2}\langle a^{\dagger}_{l\uparrow}a^{\dagger}_{l+1,\downarrow}\rangle^{*}.
\end{aligned} \tag{28}$$

The site-dependent energy of the electrons in the chain $\Delta\mu_l$ simulating the presence of diagonal disorder in the system was included in the expression for $(A_{\sigma\sigma})_{l,\,l}$. In this paper we considered the case of relatively weak diagonal disorder: $\Delta\mu_l \in [-t/2, t/2]$. The eigenvectors $\mathbf{Y}_m = (\tilde{\mathbf{u}}_{\uparrow m}, \tilde{\mathbf{u}}_{\downarrow m}, \tilde{\mathbf{v}}^{*}_{\uparrow m}, \tilde{\mathbf{v}}^{*}_{\downarrow m})^{T}$ of the Bogoliubov–de Gennes Hamiltonian (27) describe the electron-like and hole-like wave functions of a state with an excitation energy $\tilde{\varepsilon}_m$. The latter were calculated self-consistently with equilibrium correlation functions:

$$\begin{aligned}
\langle a^{\dagger}_{l\sigma}a_{l'\sigma'}\rangle &= \sum_{m=1}^{2N}[\tilde{u}_{l\sigma,m}\tilde{u}^{*}_{l'\sigma',m}f(\tilde{\varepsilon}_m/T) \\
&+ \tilde{v}_{l\sigma,m}\tilde{v}^{*}_{l'\sigma',m}(1 - f(\tilde{\varepsilon}_m/T))],
\end{aligned} \tag{29}$$

$$\begin{aligned}
\langle a^{\dagger}_{l\sigma}a^{\dagger}_{l'\sigma'}\rangle &= \sum_{m=1}^{2N}[\tilde{u}_{l\sigma,m}\tilde{v}_{l'\sigma',m}f(\tilde{\varepsilon}_m/T) \\
&+ \tilde{v}_{l\sigma,m}\tilde{u}_{l'\sigma',m}(1 - f(\tilde{\varepsilon}_m/T))].
\end{aligned} \tag{30}$$

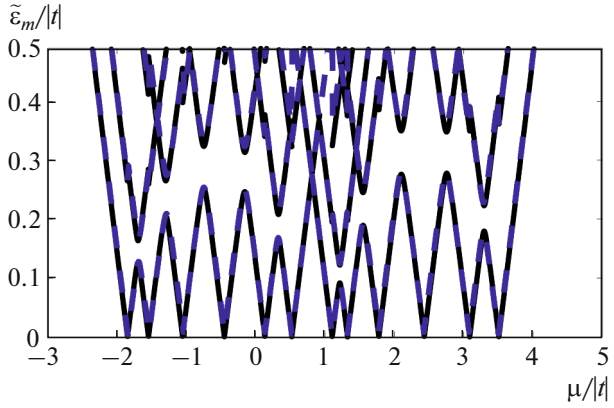


**Fig. 6.** (Color online) Dependence of the minimum excitation energies $\tilde{\varepsilon}_m$ for an open nanowire with Coulomb interactions at $n = 6$, $h = |t|$, $U = 0.5|t|$, and $V = 0.3|t|$ on chemical potential. The black dashed line represents the dependence calculated in the generalized mean-field approximation. The blue solid line represents the dependence of $\tilde{\varepsilon}_0$ found using an exact diagonalization and Lehmann's representation. $\Delta = 0.35|t|$ and $\alpha = 0.22|t|$.

For short chains ($N = 6$) a comparison of the results of our calculations obtained by the two methods described above showed that at $U, V \lesssim |t|$ the low-energy branches of the excitation spectrum $\tilde{\varepsilon}_m$ and the single-particle wave functions corresponding to them coincide to within a few percent (as demonstrated for $U = 0.5|t|$ and $V = 0.3|t|$ in Fig. 6). Accordingly, the parametric lines of change of the ground-state fermionic parity are also well reproduced in the mean-field approach.

The spectral properties, ground-state characteristics, and low-temperature thermodynamics of nanowires with a large number of sites were calculated by taking into account the Coulomb interactions in the generalized mean-field approximation. When the electron–electron interactions were taken into account, the system's peculiarities noted in previous sections turned out to be retained: for closed chains there is a parameter region for which a topologically nontrivial phase is realized. As the parameters change inside this region, a cascade of quantum transitions is realized for an open chain with a change in the ground-state fermionic parity, which is accompanied by caloric anomalies.

Examples of the fermionic parity map for an open chain and the lines of topological transitions for a closed chain for $U = 0.5|t|$ and $V = 0.3|t|$ and at the remaining parameters corresponding to Fig. 4 are presented in Fig. 7. The quantum transitions in the TNPR are seen to be retained when the interactions are taken into account; the TNPR itself can change its position in the system's phase space. Since the interaction is an electron–electron one, the regions for which the occupation numbers of single-electron

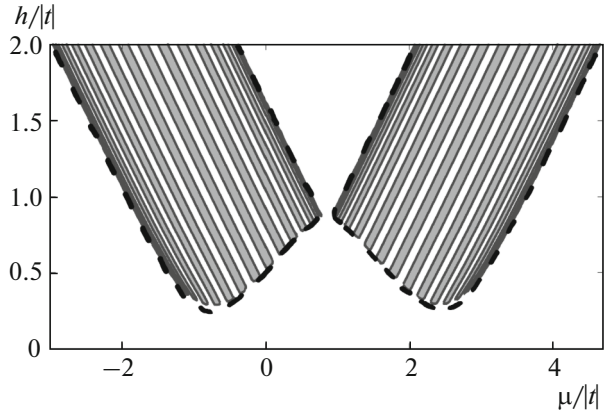


**Fig. 7.** Fermionic parity map for an open chain consisting of 30 sites and boundaries of the topological phases (dashed curves) for a closed chain when the electron correlations are taken into account: $U = 0.5|t|$ and $V = 0.3|t|$. There is no diagonal disorder ($\Delta\mu_l = 0$). The remaining parameters and color notation are the same as those in Fig. 4.

states are $\langle a^{\dagger}_{l\sigma} a_{l\sigma}\rangle \simeq 1$ are subjected to the greatest change. Figure 8a presents the field dependence of the electrocaloric effect for a nanowire with $N = 30$ and $h = 0.5|t|$. Likewise, Fig. 8b presents the field dependence of the magnetocaloric effect for a longer chain with 50 sites obtained by simultaneously taking into account the electron correlations ($U = 0.5|t|$, $V = 0.3|t|$) and diagonal disorder. The caloric anomalies are seen to be also realized in the TNPR when the electron–electron interactions, disorder, and variations in the system's sizes are taken into account.

Note that the temperatures at which the anomalies of the magneto- and electrocaloric effects manifest themselves clearly must be much lower than the characteristic gap of the bulk excitation spectrum and of the order of the characteristic edge-mode energy $\varepsilon_0$. Since $\varepsilon_0 \propto e^{-L/l_0}$, this temperature drops as the chain length increases. However, at temperatures $T \approx 20$ mK (at which a quantized differential conductance peak has been observed in recent experiments [45]) the caloric anomalies still manifest themselves clearly for chains with $N \approx 200$. Nanowires with such a length may be deemed intermediate between the limiting cases of the regime of quantum dots (to which the previous constructions refer) and the regime of long chains with well-defined Majorana fermions at the edges.

## 7. CONCLUSIONS

Our analysis showed that caloric effects are realized in a semiconductor nanowire with a strong Rashba spin–orbit interaction and proximity-induced superconductivity as the external magnetic field changes if the nanowire parameters correspond to a topologically

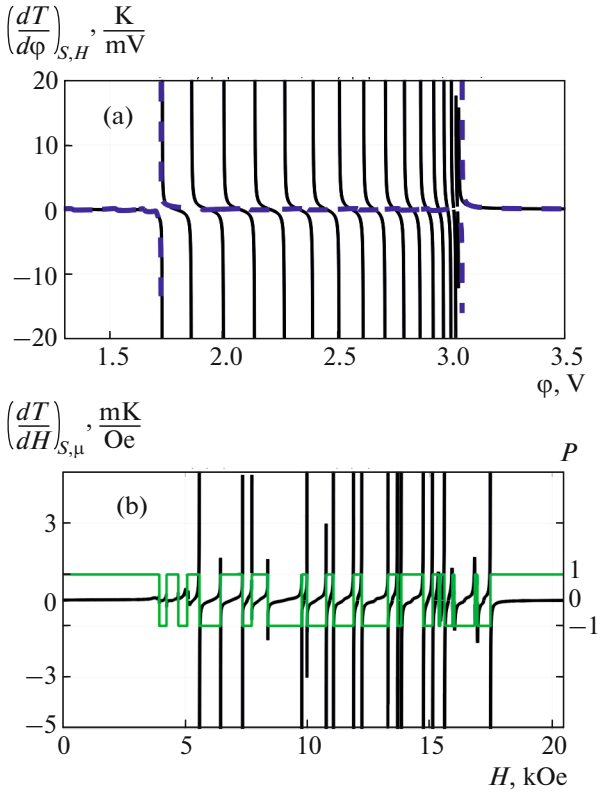


**Fig. 8.** (Color online) (a) Field dependence of the electrocaloric effect for $h = 0.5|t|$, $U = 0.5|t|$, $V = 0.3|t|$, and $\Delta\mu_l = 0$. (b) Dependence of the magnetocaloric effect on external magnetic field for a longer chain ($N = 50$) with electron–electron interactions ($U = 0.5|t|$, $V = 0.3|t|$ and in the presence of diagonal disorder $\Delta\mu_l \in [-t/2, t/2]$. The ground-state fermion parity $P$ (green line) is plotted on the right axis.

nontrivial phase determined for periodic boundary conditions. This effect can be used as an alternative method (relative to the methods proposed previously in [2, 45]) for experimentally identifying the topologically nontrivial parameter region of a nanowire. The relevance of the proposed tool for studying quantum nanowires with nontrivial properties stems from an active study of the phenomena related to the manifestation of Majorana modes in condensed matter. For practical purposes, it is important that the predicted caloric anomalies are stable with respect to the inclusion of Coulomb repulsion and diagonal disorder.

Note also that the presented effects are not restricted to a superconducting nanowire and can take place in other quasi-one-dimensional systems of symmetry class $D$, for example, such as an ensemble of electrons on a triangular lattice in the phase of coexistence of chiral superconductivity and noncollinear magnetic order considered in the geometry of a cylinder [31, 32].

## ACKNOWLEDGMENTS

We are grateful to S.V. Aksenov, A.D. Fedoseev, and A.O. Zlotnikov for their useful remarks and the discussion of our results.

## FUNDING

This work was supported by the Russian Foundation for Basic Research (project nos. 16-02-00073, 18-32-00443, 18-42-243017, 18-42-243018), the Government of the Krasnoyarsk Kray, the Krasnoyarsk Kray Science Foundation within the scientific projects "Contact Phenomena and Magnetic Disorder in the Formation and Detection of Topologically Protected Edge States in Semiconductor Nanostructures" (project no. 18-42-243018), "Manifestation of Coulomb Interactions and Bounded-Geometry Effects in the Properties of Topological Edge States of Nanostructures with Spin–Orbit Interactions" (project no. 18-42-243017). One of us (Sh. M. S.) thanks the Council for Grants of the Russian President (project nos. MK-3594.2018.2 and MK-3722.2018.2).

## REFERENCES

1. J. Alicea, Rep. Progr. Phys. **75**, 076501 (2012).
2. C. Beenakker, Ann. Rev. Condens. Matter Phys. **4**, 113 (2013).
3. T. D. Stanescu and S. Tewari, J. Phys.: Condens. Matter **25**, 233201 (2013).
4. S. R. Elliott and M. Franz, Rev. Mod. Phys. **87**, 137 (2015).
5. F. Wilczek and A. Zee, Phys. Rev. Lett. **52**, 2111 (1984).
6. S. I. Vinitskii, V. L. Derbov, V. M. Dubovik, et al., Sov. Phys. Usp. **33**, 403 (1990).
7. P. Ghosh, Jay D. Sau, S. Tewari, and S. Das Sarma, Phys. Rev. B **82**, 184525 (2010).
8. A. P. Schnyder, S. Ryu, A. Furusaki, and A. W. W. Ludwig, Phys. Rev. B **78**, 195125 (2008).
9. A. Yu. Kitaev, AIP Conf. Proc. **1134**, 22 (2009).
10. C.-K. Chiu, J. C. Y. Teo, A. P. Schnyder, and S. Ryu, Rev. Mod. Phys. **88**, 035005 (2016).
11. L. Fidkowski and A. Yu. Kitaev, Phys. Rev. B **81**, 134509 (2010).
12. V. Gurarie, Phys. Rev. B **83**, 085426 (2011).
13. Y. J. BenTov, J. High Energy Phys. **2015**, 34 (2015).
14. D. Meidan, A. Romito, and P. W. Brouwer, Phys. Rev. Lett. **113**, 057003 (2014).
15. Yi-Z. You and C. Xu, Phys. Rev. B **90**, 245120 (2014).
16. T. Morimoto, A. Furusaki, and C. Mudry, Phys. Rev. B **92**, 125104 (2015).
17. L. Fidkowski and A. Yu. Kitaev, Phys. Rev. B **83**, 075103 (2011).
18. A. M. Turner, F. Pollmann, and E. Berg, Phys. Rev. B **83**, 075102 (2011).
19. F. Pollmann, A. M. Turner, E. Berg, and M. Oshikawa, Phys. Rev. B **81**, 064439 (2010).
20. X. Chen, Z.-C. Gu, and X.-G. Wen, Phys. Rev. B **83**, 035107 (2011).
21. N. Schuch, D. Perez-Garcia, and I. Cirac, Phys. Rev. B **84**, 165139 (2011).
22. F. Pollmann, E. Berg, A. M. Turner, and M. Oshikawa, Phys. Rev. B **85**, 075125 (2012).
23. N. Read and D. Green, Phys. Rev. B **61**, 10267 (2000).
24. A. Y. Kitaev, Phys. Usp. **44**, 131 (2001).
25. L. Fu and C. L. Kane, Phys. Rev. Lett. **100**, 096407 (2008).
26. J. D. Sau, R. M. Lutchyn, S. Tewari, and S. Das Sarma, Phys. Rev. Lett. **104**, 040502 (2010).
27. J. D. Sau, S. Tewari, R. M. Lutchyn, et al., Phys. Rev. B **82**, 214509 (2010).
28. R. M. Lutchyn, J. D. Sau, and S. Das Sarma, Phys. Rev. Lett. **105**, 077001 (2010).
29. A. Yu. Kitaev, Ann. Phys. **321**, 2 (2006).
30. I. Martin and A. F. Morpurgo, Phys. Rev. B **85**, 144505 (2012).
31. Y.-M. Lu and Z. Wang, Phys. Rev. Lett. **110**, 096403 (2013).
32. V. V. Val'kov, A. O. Zlotnikov, and M. S. Shustin, J. Magn. Magn. Mater. **459**, 112 (2018).
33. V. Aleshkin, V. Gavrilenko, A. Ikonnikov, et al., Semiconductors **42**, 828 (2008).
34. H. A. Nilsson, P. Caroff, C. Thelander, et al., Nano Lett. **9**, 3151 (2009).
35. M. T. Deng, S. Vaitiekenas, E. B. Hansen, et al., Science (Washington, DC, U. S.) **354**, 1557 (2016).
36. J. Alicea, Y. Oreg, G. Refael, et al., Nat. Phys. **7**, 412 (2011).
37. D. J. Clarke, J. D. Sau, and S. Tewari, Phys. Rev. B **84**, 035120 (2011).
38. B. van Heck, A. R. Akhmerov, F. Hassler, et al., New J. Phys. **14**, 035019 (2012).
39. B. I. Halperin, Y. Oreg, A. Stern, et al., Phys. Rev. B **85**, 144501 (2012).
40. S. Nadj-Perge, I. K. Drozdov, B. A. Bernevig, and A. Yazdani, Phys. Rev. B **88**, 020407(R) (2013).
41. S. Nadj-Perge, I. K. Drozdov, J. Li, et al., Science (Washington, DC, U. S.) **346**, 602 (2014).
42. F. Zhang, C. L. Kane, and E. J. Mele, Phys. Rev. Lett. **111**, 056402 (2013).
43. A. Keselman, L. Fu, A. Stern, and E. Berg, Phys. Rev. Lett. **111**, 164402 (2013).
44. V. Mourik, K. Zuo, S. M. Frolov, et al., Science (Washington, DC, U. S.) **336**, 1003 (2012).
45. R. M. Lutchin, E. P. A. Bakkers, L. P. Kouwenhoven, et al., Nat. Rev. Mater. **3**, 52 (2018).
46. S. R. Elliott and M. Franz, Rev. Mod. Phys. **87**, 137 (2015).
47. C. Moore, C. Zeng, T. D. Stanescu, and S. Tewari, Phys. Rev. B **98**, 155314 (2018).
48. C. Zeng, C. Moore, A. M. Rao, et al., arXiv: 1808.02495 (2018).
49. C. Reeg, D. Loss, and J. Klinovaja, Phys. Rev. B **96**, 125426 (2017).
50. G. W. Winkler, D. Varjas, R. Skolasinski, et al., Phys. Rev. Lett. **119**, 037701 (2017).
51. E. M. Stoudenmire, J. Alicea, O. A. Starykh, and M. P. A. Fisher, Phys. Rev. B **84**, 014503 (2011).

52. S. Gangadharaiah, B. Braunecker, P. Simon, and D. Loss, Phys. Rev. Lett. **107**, 036801 (2011).
53. O. Motrunich, K. Damle, and D. A. Huse, Phys. Rev. B **63**, 224204 (2001).
54. P. W. Brouwer, M. Duckheim, A. Romito, and F. von Oppen, Phys. Rev. B **84**, 144526 (2011).
55. D. Rainis, L. Trifunovic, J. Klinovaja, and D. Loss, Phys. Rev. B **87**, 024515 (2013).
56. F. Crepin, G. Zarand, and P. Simon, Phys. Rev. B **90**, 121407(R) (2014).
57. N. Sedlmayr and C. Bena, Phys. Rev. B **92**, 115115 (2015).
58. N. Sedlmayr, J. M. Aguiar-Hualde, and C. Bena, Phys. Rev. B **93**, 155425 (2016).
59. O. Dmytruk and J. Klenovaja, arXiv:1710.01671v1 (2017).
60. F. Pientka, A. Romito, M. Duckheim, et al., New J. Phys. **15**, 025001 (2013).
61. A. A. Zvyagin, Low Temp. Phys. **41**, 806 (2015).
62. S. Hegde and S. Vishveshwara, Phys. Rev. B **94**, 115166 (2016).
63. N. M. Gergs, L. Fritz, and D. Schuricht, Phys. Rev. B **93**, 075129 (2016).
64. H. Katsura, D. Schuricht, and M. Takahashi, Phys. Rev. B **92**, 115137 (2015).
65. J.-J. Miao, H.-K. Jin, F.-C. Zhang, and Y. Zhou, Phys. Rev. Lett. **118**, 267706 (2017).
66. V. V. Val'kov, V. A. Mitskan, and M. S. Shustin, JETP Lett. **106**, 798 (2017).
67. J. C. Budich and E. Ardonne, Phys. Rev. B **88**, 075419 (2013).
68. A. D. Fedoseev, J. Exp. Theor. Phys. **128**, 125 (2019).
69. L. Zhu, M. Garst, A. Rosch, and Q. Si, Phys. Rev. Lett. **91**, 066404 (2003).
70. M. Garst and A. Rosch, Phys. Rev. B **72**, 205129 (2005).
71. V. V. Val'kov, M. Yu. Kagan, and S. V. Aksenov, arXiv:1809.09222.
72. H. Lehmann, Nuovo Cim. **11**, 342 (1954).
73. B. G. Kukharenko, Sov. Phys. JETP **42**, 321 (1975).
74. V. V. Val'kov and T. A. Val'kova, Sov. Phys. JETP **72**, 1053 (1991).

*Translated by V. Astakhov*